# Generation of Mode-Reconfigurable and Frequency-Adjustable OAM Beams Using Dynamic Reflective Metasurface

**KAI GUO[1], QUN ZHENG[1,2,3], ZHIPING YIN [1,2,3], (Member, IEEE), AND ZHONGYI GUO [1,2,3]**

[1]School of Computer and Information, Hefei University of Technology, Hefei 230009, China
[2]Academy of Photoelectric Technology, Hefei University of Technology, Hefei 230009, China
[3]School of Electronics Science and Applied Physics, Hefei University of Technology, Hefei 230009, China

Corresponding authors: Zhiping Yin (zpyin@hfut.edu.cn) and Zhongyi Guo (guozhongyi@hfut.edu.cn)

**ABSTRACT** Recently, much attention has been paid to beams carrying orbital angular momentum (OAM) for radio communication, which faces a great challenge of dynamic generation of OAM with different topological charges. In this paper, a novel reflective metasurface is designed to generate mode-reconfigurable OAM beams in radio frequency domain. Each unit cell of the proposed metasurface consists of an octagonal ring slot and a varactor diode. The response of each element to incident radio field can be engineered individually by controlling the voltage of the corresponding varactor diode, thereby dynamically producing OAM with different modes. Full-wave simulations show that the designed reflective metasurface can generate frequency-adjustable OAM beams with different topological charges of $l = +1, +2, -1, -2$ over a frequency range of 5.2 GHz$\sim$5.8 GHz. An OAM purity analysis further verified the reliability of OAM beams generated by the proposed metasurface. The obtained results are in good agreements with the theoretical analyses, demonstrating a good prospect of practical application.

## I. INTRODUCTION

In 1992, Allen *et al.* first found the fact that the Laguerre-Gaussian (LG) light beams can carry a certain mode of orbital angular momentum (OAM) [1], and proposed that light beams with a helical phase front have the potential to benefit the relevant applications in optical manipulation. In addition, OAM modes are orthogonal to each other, making it possible to increase the channel capacity of wireless communication system without additional frequency resources [2], [3]. In the past decades, the OAM vortex beam has become an important research topic due to its excellent physical nature and the potential applications [4]–[9]. In 2007, Thidé extended the investigations on OAM from optics to microwave and proposed to generate OAM using phased array antennas [10], promoting the development of OAM in microwave communication [11].

A variety of methods have been reported to generate OAM vortex waves in microwave range, including spiral phase

The associate editor coordinating the review of this manuscript and approving it for publication was Giovanni Angiulli.

plate (SPP) [12] and phased array antenna [13]–[18]. The structure of SPP is simple, but it can only obtain the OAM beam with a single mode, restricting the practical application. In addition, it is not easy to precisely fabricate a SPP with a screwed structure, resulting in the divergence and mode purity reduction of generated OAM beam. The circular phased array antenna could precisely control the phase distribution and generate OAM mode with high purity. However, it usually needs to employ complex feeding network with phase shifters, and the gain is not high due to the loss of complicated feeding circuits. To solve these problems, there have been some new ways to generate OAM vortex waves such as holographic plate [19], travel-wave antenna [20]–[24] and dielectric resonator antenna [25], [26]. Holographic plate and dielectric resonator antenna can produce OAM beams with small divergence angle, but they have relatively low gains. The circular travel-wave antenna can generate multiple OAM modes simultaneously, but it has large size and high profile. Very recently, metasurface has been introduced to microwave range to generate OAM beams owing to its advantages such as low profile, high gain, and flexible

capability of modulating electromagnetic waves [27]–[38]. However, the previous studies of microwave metasurface rarely produced OAM beams possessing the characteristics of reconfigurable mode and adjustable working frequency simultaneously, which greatly hinders its applications.

In this paper, we propose a novel reflective metasurface to generate mode-reconfigurable and frequency-adjustable OAM beams in microwave range. Each unit cell of the proposed reflective metasurface can actively engineer the phase profile by a varactor diode. The proposed metasurface is illuminated by a horn antenna and introduces an azimuthal phase profile of $e^{jl\varphi}$ ($\varphi$ is the azimuthal angle) into the reflect electromagnetic waves, generating vortex waves. Numerical simulation results show that the proposed reflective metasurface can generate mode-reconfigurable OAM beams with high purities in the bandwidth. Our proposed method has potential application in future wireless communication system.
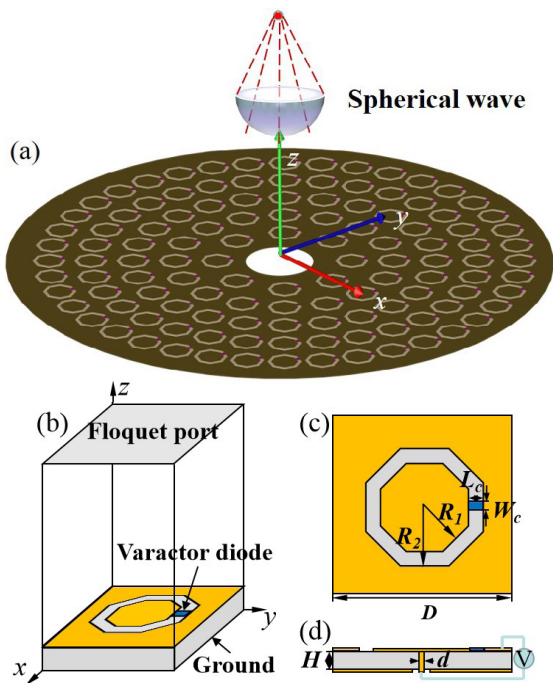


**FIGURE 1.** (a) Schematic model of the reflective metasurface for OAM generation. (b) Schematic diagram of the proposed element. (c) Top view and (d) Side view of the proposed element.

## II. PRINCIPLE AND DESIGN OF REFLECTIVE METASURFACE

Figure 1(a) schematically shows the proposed reflective metasurface, which is normally illuminated by a horn antenna and transform the incident waves into reflected OAM vortex waves. The substrate of the metasurface is TMM13i with dielectric constant of $\varepsilon_r = 12.2$, loss tangent of $\tan\delta = 0.0019$, and thickness of 1.5 mm. The substrate with high dielectric constant can be helpful to miniaturization of the structure since higher dielectric constant results in lower resonant frequency [39]. Considering the specific phase profile

of vortex beam and the cost, the metasurface totally consists 120 units arranged in five circles. From inner to outer, these circles has radius of 20 mm, 30 mm, 40 mm, 50 mm and 60 mm, and contains 8, 16, 24, 32, and 40 uniformly distributed unit elements, respectively. Our design can be read from Fig. 1(a). Therefore, to simplify the structure and avoid disturbing, the structure is designed as a ring, whose inner and outer radius is 15 mm and 70 mm, respectively. It is because that space of the central part of the metal plate is not enough to accommodate unit elements for OAM beam generation, and the reflected field from this area will interfere with that from unit elements, disturbing the generated OAM beam.

**TABLE 1.** Parameters of the unit element.

| Parameters | $R_1$ | $R_2$ | $L_c$ | $W_c$ | $D$ | $d$ | $H$ |
|---|---|---|---|---|---|---|---|
| Unit/mm | 3.6 | 4.4 | 0.8 | 0.4 | 10 | 1.3 | 1.5 |

To ensure the metasurface working at frequency range of 4.5GHz~6.5GHz, the geometric parameters have been numerically optimized. The unit structure of the proposed metasurface is shown in Fig. 1(b-d) and its parameters are given in Table 1. In the top layer, an octagonal slot is cut into a metal patch, and a varactor diode is inserted into the slot to connect the inner and outer metal patches. Note that we choose octagonal ring rather than circular and square rings since octagonal ring slot is more feasible to insert varactor diode than the circular case and provides larger reflection area of antenna than the square case. The inner metal patch is connected to a metal column through a via inside the substrate, through changing the voltage applied between the metal column and the outer metal patch, the diode capacitance can be well controlled. The metal column is not connected to the bottom ground, therefore we can manipulate the varactor diode individually by using the field programmable gate array (FPGA). This method minimizes the outer disturbing on the reflection field. As a result, the capacitance of the varactor diode can be changed by applying a voltage to the inner and outer metal patches, therefore changing the responses of metasurface to incident electromagnetic field. This concept may allow us to dynamically engineer the phase distribution of reflective field and generate mode-reconfigurable OAM beams with a unique metasurface.

To demonstrate, simulation models of the designed element are built by using a commercial software High Frequency Structure Simulator (HFSS) which is based on the finite element method. In the simulations, the floquet port excitation is adopted as the incident source and perfect electrical conductor condition is used as ground, as shown in Fig. 1(b). To simulate the response of each unit element, master–slave boundary condition is set at the boundaries in both *x*- and *y*-direction to save the computing memory and time. To simulate the designed metasurface, radiative boundary condition is used in horizontal boundaries instead. We set incident source as a spherical wave with *y*-polarization, which can be generated by Vivaldi antenna and horn antennas in

microwave regime [29], [30]. This kind of source will not block the reflection aperture. In our design, the parameter of varactor diode is chosen as MAVR-000120-1411 from MACOM [40], whose capacitance value ranges from 0.14 pF to 1.1 pF. In the simulation, we consider an ideal case and the capacitance value is described by an equivalent RLC boundary, in which the resistance and inductance are not taken into consideration. Even though loss from resistance may affect the reflected wave, luckily, it has been demonstrated that its influence on reflection phase can be negligible [41]. The unit element, which is composed of the octagonal slot, metal patch, and varactor, can be represented with an equivalent LC circuit. The metallic part and varactor can be modeled by inductance $L$ and capacitance $C$, respectively. The load impedance can be calculated by $Z_{eff} = jwL + 1/jwC$. By utilizing the tunable capacitance of varactor, we can manipulate the load impedance to create different surface impedance of the unit element. It is known that the electromagnetic response can be described by the impedance $Z_S$ as $\vec{E} = Z_S \left( \hat{n} \times \vec{H} \right)$, where $\hat{n}$ is a unit vector. Thus, the capacitance value changes the surface impedance of the unit element, providing us with an opportunity to engineer the reflected electric field. In this method, the radio-frequency performance can be dynamically altered through simple low-cost bias voltage, and the coupling between investigated radio-frequency and dc voltages is negligible [35], [39].
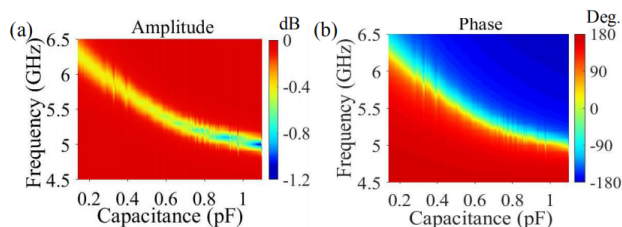


**FIGURE 2.** Simulated (a) magnitude and (b) phase of reflection coefficient for the unit element with different capacitance values from 0.14 pF to 1.1 pF.

Figure 2 shows the simulated magnitude and phase of reflected wave from a unit element as functions of varactor diode capacitance and incident frequency. Note that, we are trying to achieve mode-reconfigurable OAM beams by using varactor diode. Thus, it is not considered to change the geometry parameters, such as the position and size of the varactor diodes. Instead, we dynamically tune the capacitance value of the varactor diode from 0.14 pF to 1.1 pF and the incident frequency is over a broadband range from 4.5 GHz to 6.5 GHz. It can be seen from Fig. 2(a) that the amplitude changes abruptly at specific frequency when the capacitance value changes, indicating the unit element could resonantly interact with the incident electromagnetic field at this frequency. In addition, the resonance frequency decreases as the capacitor value increases. It means that interaction between the unit element and the incident field will change when the capacitance has different value, and it may result in phase

shift of reflected wave at fixed frequency. Figure 2(b) shows that the reflected phase could shift from 0 to $2\pi$ by controlling the capacitances of varactor diode, which could satisfy the requirement of OAM beams generation. According to these results, we choose 5.2 GHz to 5.8 GHz for two reasons: first, variation of the reflected amplitude is smaller than 0.5 dB in this frequency range when the capacitance changes; second, beyond this range it either cannot cover entire phase shift of 0-$2\pi$ or is difficult to precisely control the capacitance. Similar experiment of precisely controlling the capacitance value of varactor can be referred to [41].

To generate an OAM beam, the phase distribution at metasurface generally consists of two parts: one is the helical phase distribution of the form $e^{jl\varphi}$ along the azimuthal axis, where $l$ represents the topological charge of an OAM beam, and the other one is the compensation for the phase of incident wave, which is determined by the source. In our case, the phase shift could be represents by [31], [33]

$$\varphi(x, y) = l \cdot \arctan\left(\frac{x}{y}\right) - \frac{2\pi}{\lambda_0} r_{xy} \qquad (1)$$

where $(x, y)$ is the coordinate in the metasurface plane, $\lambda_0$ is the wavelength in vacuum, $r_{xy}$ is the distance from the center of horn to the location $(x, y)$. Here, the incident spherical wave is 75 mm away from the metasurface. The phase value of compensation for each unit element can be calculated. Figures 3(a-d) show the phase distributions of the designed metasurface to generate OAM beam with topological charge of $l = -1, +1, -2, +2$, respectively, which are calculated from Eq. (1). In the following, we demonstrate the performance of the proposed metasurface to generate mode-reconfigurable OAM beams.
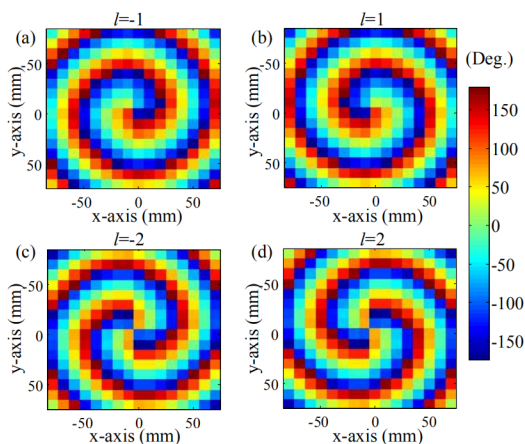


**FIGURE 3.** Phase distributions of the reflective metasurface to generate OAM mode with topological charge of (a) l = −1, (b) l = +1, (c) l = −2, (d) l = +2.

## III. RESULTS AND DISCUSSION

As discussed above, the reflected phase response of the proposed structure varies with the capacitance and the results in Fig. 2 suggests us to generate OAM beams in the frequency

ranging from 5.2 GHz to 5.8 GHz. Therefore, a reconfigurable OAM mode can be effectively achieved by the metasurface through electrically controlling the capacitance of varactor diodes.
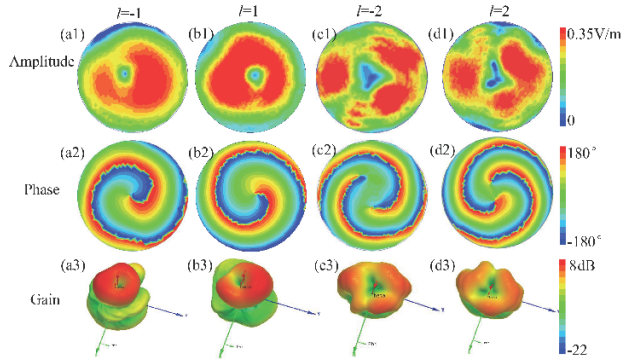


**FIGURE 4.** The electric field intensity (a1)-(d1), phase distributions (a2)-(d2), and far-field radiation patterns of the generated OAM beams in x-y plane with topological charge of l = −1, +1, −2 and +2 (from left to right). In these cases, the designed metasurface works at frequency of 5.2 GHz. The observation plane is 300 mm away from metasurface.

Figure 4 shows the simulation results of the generated OAM beams with topological charges of $l = -1, +1, -2$ and $+2$ (from left to right) at frequency of 5.2 GHz by electrically tuning the varactor diode. Figures 4(a1)-(d1) show the amplitude distributions of electric field in $x$-$y$ plane, which is observed in a circle with radius of 250 mm at a distance of 300 mm (about 5 times of wavelength) from the metasurface. These generated electric field exhibit the characteristics of OAM beams with ring-like amplitude distributions, which are caused by phase singularity at the central region. In addition, the central dark zone grows larger when the topological charge $l$ of the OAM beam increases. The non-uniformly distributed amplitude may be attributed to the difference in reflected amplitude between unit elements in the designed metasurface. The features of spiral phase distribution are also obvious. As shown in Figs. 4(a2)-(d2), the phase variation of $-2\pi, 2\pi, -4\pi$ and $4\pi$, respectively, happens in a circle along the azimuthal direction, which also confirms the characteristics of OAM beam. Figures 4(a3)-(d3) show the corresponding far-field radiation patterns with amplitude nulls existing at the central regions. From both the near-field and far-field performances, it is found that the major feature of the OAM beam is successfully obtained, and different OAM modes can be dynamically achieved, verifying the good performance of the mode reconfiguration.

As mentioned above, this proposed metasurface has another advantage of frequency-adjustable characteristic. To demonstrate, we simulate the generation of OAM beams with topological charges of $l = -1, +1, -2$ and $+2$ at frequency of 5.8 GHz, as shown in Fig. 5 (from left to right). It is also observed in $x$-$y$ plane within a circle with radius of 250 mm at a distance of 300 mm (about 6 times of wavelength) from the metasurface. It can be seen that the results are similar to the case of 5.2 GHz, exhibiting the key features
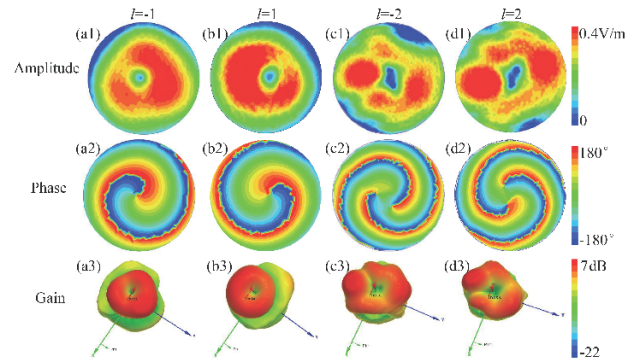


**FIGURE 5.** The electric field intensity (a1)-(d1), phase distributions (a2)-(d2), and far-field radiation patterns of the generated OAM beams in x-y plane with topological charge of l = −1, +1, −2 and +2 (from left to right). In these cases, the designed metasurface works at frequency of 5.8 GHz.

of OAM beam. The top and bottom panels show ring-like amplitude distributions with central nulls which are attributed to phase singularity at the centers in $x$-$y$ plane. The size of the central nulls increases when the absolute value of topological charge becomes larger. In addition, the middle panel shows the feature of spiral phase distributions changing from 0 to $-2\pi, 2\pi, -4\pi$ and $4\pi$ (from left to right) in a circle along the azimuthal direction. Overall, we obtained a very good result demonstrating the good performance of the proposed method to generate mode-reconfigurable OAM beams with adjustable working frequency in microwave range.

To further verify the reliability of the proposed method, the power spectrum of these OAM beams generated by the designed metasurface is calculated using the discrete Fourier transform algorithm. The Fourier relationship between the OAM spectrum $P(\alpha)$ and the corresponding sampling phase $\psi(\varphi)$ can be expressed as [22]

$$\psi(\varphi) = \sum_{-\infty}^{+\infty} P(\alpha) \exp(jl\varphi) \qquad (2)$$

$$P(\alpha) = \frac{1}{2\pi} \int_0^{2\pi} \psi(\varphi) \exp(-jl\varphi) \, d\varphi \qquad (3)$$

where $\psi(\varphi)$ refers to the discrete sampling phase value in the sampling plane, exp($-jl\varphi$) is the harmonic related to the spiral phase front.

We simulated the generation of OAM beams with topological charges of $l = +1, -1, +2$, and $-2$ at frequencies of 5.2 GHz, 5.4 GHz, 5.6 GHz and 5.8 GHz and calculated the power spectra. In these cases, the propagation distance of OAM beams is set to be 300 mm (about 5~6 times of wavelength), and the radius of a circular observation area is 150mm. The chosen area is the main radiation direction of wave propagation, so the model purity is most accurate in this area. As shown in Figs. 6(a)-(d), the power spectra of the generated OAM beam with topological charges of $l = -1, +1, -2$, and $+2$ are calculated at the frequencies of 5.2GHz, 5.4 GHz, 5.6 GHz and 5.8 GHz. It can be seen that most of the power is concentrated within the generated OAM
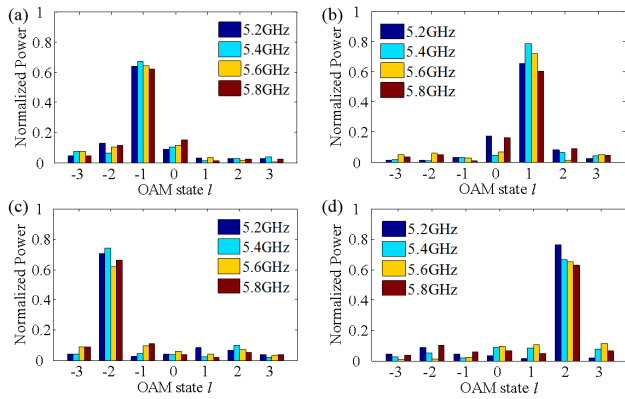
**FIGURE 6.** Histograms of OAM spectrum weight at different frequencies of 5.2 GHz, 5.4 GHz, 5.6 GHz and 5.8 GHz. The generated topological charge of OAM beam from metasurface is (a) l = −1, (b) l = +1, (c) l = −2, (d) l = +2, respectively.



**FIGURE 7.** Mode purity of generated OAM beams with l = +1, −1, +2 and −2 at the frequencies ranging from 5.2 GHz to 5.8 GHz.

**TABLE 3.** Comparison between the proposed scheme with previous results.

| Ref. | Type | $f_0$(GHz) | Bandwidth | OAM | Purity | Gain(dBi) | Method |
|------|------|--------|-----------|-----|--------|-----------|--------|
| [2] | Patch | 5.65 | Narrow | -2,1 | N.A. | N.A. | Exp. |
| [12] | SPP | 0.03 | Narrow | 1 | N.A. | 8.5 | Sim. |
| [14] | Phase Array | 9.90 | Narrow | 0-7 | N.A. | N.A. | Exp. |
| [15] | Antenna Array | 5.80 | 5.72-5.95 | ±1 | N.A. | N.A. | Exp. |
| [16] | Antenna Array | 5.50 | 5.39-5.69 | ±1 | N.A. | N.A. | Exp. |
| [18] | Patch Array | 2.47 | Narrow | ±1 | ≥0.90 | 4.8 | Exp. |
| [20] | Antenna | 10 | Narrow | ±3 | N.A. | 3.71 | Exp. |
| [27] | Metasurface | 5.80 | Narrow | 1,2,4 | N.A. | N.A. | Exp. |
| [30] | Reflectarray | 6, 10 | Narrow | ±1 | ≥0.62 | 17.7 | Exp. |
| [33] | Metasurface | 8.50 | Narrow | ±1, ±2 | N.A. | N.A. | Exp. |
| Us | Metasurface | 5.50 | 5.20-5.80 | ±1, ±2 | >0.60 | 7~8 | Sim. |

mode, meanwhile, there is part of the power extending to the neighboring OAM channels. It is in a good agreement with the result of field distributions above.

From the experimental point of view, the fabrication inaccuracies, for example the capacitance error, may have influence on the generated OAM beams. It is because the phase of reflected wave highly depends on the capacitance values, especially around the resonance frequencies. To demonstrate, we performed simulations at frequency of 5.8GHz, randomly selecting half of the unit elements and introducing errors to their capacitance values. When the error is 0.02pF, the mode purities of OAM beams with $l = −1, 1, −2$ and 2 are calculated to be $0.60, 0.61, 0.63$, and $0.59$, in contrast, the corresponding mode purities of ideal cases are $0.62, 0.64, 0.68$, and $0.65$, respectively. By optimizing the capacitance values in experiment, the fabrication errors may be compensated and the generated OAM beam can be improved.

We additionally studied the mode purities of these OAM beams at frequency of 5.2GHz with propagation distances of 200mm, 250mm and 300mm, as summarized in Table 2. Due to the divergence of OAM beam, the observation area varies to ensure most of the energy can be involved. It can be seen that the calculated mode purities do not vary significantly with the propagation distance. In addition, the mode purities of OAM beams with $l = ±1$ are more stable than that with $l = ±2$ since the divergence is more obvious for the latter cases.

**TABLE 2.** Purity as function of propagation distance at 5.2GHZ.

| Distance | l=-1 | l=1 | l=-2 | l=2 |
|----------|------|-----|------|-----|
| 200mm | 0.60 | 0.65 | 0.63 | 0.64 |
| 250mm | 0.61 | 0.64 | 0.74 | 0.76 |
| 300mm | 0.62 | 0.60 | 0.61 | 0.62 |

Because different capacitance values bring changes in both phase and amplitude of reflection, resulting in difference in reflected amplitude between unit elements in the
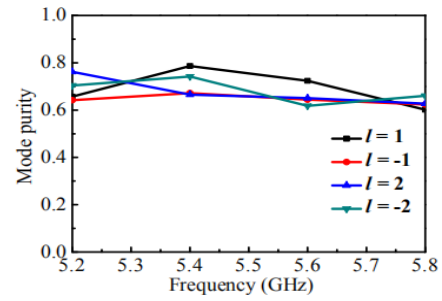
designed metasurface, and finally leading to the mode impurity. Fortunately, the calculated spectrum purities for all generated OAM modes are higher than 60% at all frequencies, as summarized in Fig. 7. Therefore, it is demonstrated further that proposed method could dynamically generate the OAM beams with good purity over the frequency range of 5.2 GHz~5.8 GHz.

Table 3 summarizes different techniques to compare the results of our proposed scheme with that of the other state-of-the-art techniques. From the view of mode purity, our scheme are comparable with the state-of-the-art techniques. While considering the mode-reconfigurable and frequency-tunable properties, our results are better than most reported cases.

## IV. CONCLUSION

In conclusion, we propose a novel reflective metasurface with varactor diodes, which can generate mode-reconfigurable and frequency-adjustable OAM beam in microwave range by tuning the capacitance of varactor diode. Simulation results demonstrated that the designed reflective metasurface can generate OAM mode of $l = −1, −2, +1$ and $+2$ with mode purity over 60% in the frequency ranging from 5.2 GHz to 5.8 GHz. The proposed reflective metasurface has the advantages of small size, low profile, mode reconfiguration and

frequency-adjustable characteristics, which has great importance in future wireless communications system.

## REFERENCES

[1] L. Allen, M. W. Beijersbergen, R. J. C. Spreeuw, and J. P. Woerdman, "Orbital angular momentum of light and the transformation of Laguerre–Gaussian laser modes," *Phys. Rev. A, Gen. Phys.*, vol. 45, no. 11, pp. 8185–8189, Jun. 1992.

[2] Z. Zhang, S. Xiao, Y. Li, and B.-Z. Wang, "A circularly polarized multimode patch antenna for the generation of multiple orbital angular momentum modes," *IEEE Antennas Wireless Propag. Lett.*, vol. 16, pp. 521–524, 2017.

[3] S. Zheng, W. Zhang, Z. Zhang, X. Jin, H. Chi, and X. Zhang, "Generation and propagation characteristics of electromagnetic vortices in radio frequency," *Photon. Res.*, vol. 4, no. 5, pp. B9–B13, Oct. 2016.

[4] D. G. Grier, "A revolution in optical manipulation," *Nature*, vol. 424, no. 6950, pp. 810–816, Aug. 2003.

[5] Z. Wang and Z. Guo, "Adaptive demodulation technique for efficiently detecting orbital angular momentum (OAM) modes based on the improved convolutional neural network," *IEEE Access*, vol. 7, pp. 163633–163643, 2019.

[6] G. C. G. Berkhout and M. W. Beijersbergen, "Method for probing the orbital angular momentum of optical vortices in electromagnetic waves from astronomical objects," *Phys. Rev. Lett.*, vol. 101, no. 10, Sep. 2008, Art. no. 100801.

[7] Z. Guo, Z. Wang, M. I. Dedo, and K. Guo, "The orbital angular momentum encoding system with radial indices of Laguerre–Gaussian beam," *IEEE Photon. J.*, vol. 10, no. 5, Jul. 2018, Art. no. 7906511.

[8] Z. Feng, X. Wang, M. I. Dedo, K. Guo, F. Shen, C. Kai, and Z. Guo, "High-density orbital angular momentum mode analyzer based on the mode converters combining with the modified Mach–Zehnder interferometer," *Opt. Commun.*, vol. 435, pp. 441–448, Mar. 2019.

[9] Z. Wang, M. I. Dedo, K. Guo, K. Zhou, F. Shen, Y. Sun, S. Liu, and Z. Guo, "Efficient recognition of the propagated orbital angular momentum modes in turbulences with the convolutional neural network," *IEEE Photon. J.*, vol. 11, no. 3, Jun. 2019, Art. no. 7903614.

[10] B. Thidé, H. Then, J. Sjöholm, K. Palmer, J. Bergman, T. D. Carozzi, Y. N. Istomin, N. H. Ibragimov, and R. Khamitova, "Utilization of photon orbital angular momentum in the low-frequency radio domain," *Phys. Rev. Lett.*, vol. 99, no. 8, Aug. 2007, Art. no. 087701.

[11] Y. Yan, G. Xie, M. P. J. Lavery, H. Huang, N. Ahmed, C. Bao, Y. Ren, Y. Cao, L. Li, Z. Zhao, A. F. Molisch, M. Tur, M. J. Padgett, and A. E. Willner, "High-capacity millimetre-wave communications with orbital angular momentum multiplexing," *Nature Commun.*, vol. 5, no. 1, Dec. 2014, Art. no. 4876.

[12] S. M. Mohammadi, L. K. Daldorff, J. E. Bergman, R. L. Karlsson, B. Thidé, K. Forozesh, and B. Isham, "Orbital angular momentum in radio—A system study," *IEEE Trans. Antennas Propag.*, vol. 58, no. 2, pp. 565–572, Mar. 2009.

[13] Z. Guo, Y. Wang, Q. Zheng, C. Yin, Y. Yang, and Y. Gong, "The progresses on the antenna technologies of the vortex electromagnetic wave," *J. Radars*, vol. 8, no. 5, pp. 631–655, Oct. 2019.

[14] K. Liu, H. Liu, Y. Qin, Y. Cheng, S. Wang, X. Li, and H. Wang, "Generation of OAM beams using phased array in the microwave band," *IEEE Trans. Antennas Propag.*, vol. 64, no. 9, pp. 3850–3857, Sep. 2016.

[15] Z.-G. Guo and G.-M. Yang, "Radial uniform circular antenna array for dual-mode OAM communication," *IEEE Antennas Wireless Propag. Lett.*, vol. 16, pp. 404–407, 2017.

[16] H. Li, L. Kang, F. Wei, Y.-M. Cai, and Y.-Z. Yin, "A low-profile dual-polarized microstrip antenna array for dual-mode OAM applications," *IEEE Antennas Wireless Propag. Lett.*, vol. 16, pp. 3022–3025, 2017.

[17] B. Liu, Y. Cui, and R. Li, "A broadband dual-polarized dual-OAM-mode antenna array for OAM communication," *IEEE Antennas Wireless Propag. Lett.*, vol. 16, pp. 744–747, 2017.

[18] C. Guo, X. Zhao, C. Zhu, P. Xu, and Y. Zhang, "An OAM patch antenna design and its array for higher order OAM mode generation," *IEEE Antennas Wireless Propag. Lett.*, vol. 18, no. 5, pp. 816–820, May 2019.

[19] F. Tamburini, E. Mari, A. Sponselli, B. Thidé, A. Bianchini, and F. Romanato, "Encoding many channels on the same frequency through radio vorticity: First experimental test," *New J. Phys.*, vol. 14, no. 3, 2012, Art. no. 033001.

[20] Z. Zhang, S. Zheng, X. Jin, H. Chi, and X. Zhang, "Generation of plane spiral OAM waves using traveling-wave circular slot antenna," *IEEE Antennas Wireless Propag. Lett.*, vol. 16, pp. 8–11, 2017.

[21] W. Zhang, S. Zheng, X. Hui, Y. Chen, X. Jin, H. Chi, and X. Zhang, "Four-OAM-mode antenna with traveling-wave ring-slot structure," *IEEE Antennas Wireless Propag. Lett.*, vol. 16, pp. 194–197, 2017.

[22] F. Shen, J. Mu, K. Guo, and Z. Guo, "Generating circularly polarized vortex electromagnetic waves by the conical conformal patch antenna," *IEEE Trans. Antennas Propag.*, vol. 67, no. 9, pp. 5763–5771, Sep. 2019.

[23] F. Shen, J. Mu, K. Guo, S. Wang, and Z. Guo, "Generation of continuously variable-mode vortex electromagnetic waves with three-dimensional helical antenna," *IEEE Antennas Wireless Propag. Lett.*, vol. 18, no. 6, pp. 1091–1095, Jun. 2019.

[24] L. Wang, H. Chen, K. Guo, F. Shen, and Z. Guo, "An inner- and outer-fed dual-arm archimedean spiral antenna for generating multiple orbital angular momentum modes," *Electronics*, vol. 8, no. 2, 2019, Art. no. 251.

[25] J. Liang and S. Zhang, "Orbital angular momentum (OAM) generation by cylinder dielectric resonator antenna for future wireless communications," *IEEE Access*, vol. 4, pp. 9570–9574, 2016.

[26] Y. Pan, S. Zheng, J. Zheng, Y. Li, X. Jin, H. Chi, and X. Zhang, "Generation of orbital angular momentum radio waves based on dielectric resonator antenna," *IEEE Antennas Wireless Propag. Lett.*, vol. 16, pp. 385–388, 2017.

[27] S. Yu, L. Li, G. Shi, C. Zhu, X. Zhou, and Y. Shi, "Design, fabrication, and measurement of reflective metasurface for orbital angular momentum vortex wave in radio frequency domain," *Appl. Phys. Lett.*, vol. 108, no. 12, Mar. 2016, Art. no. 121903.

[28] M. L. N. Chen, L. J. Jiang, and W. E. I. Sha, "Detection of orbital angular momentum with metasurface at microwave band," *IEEE Antennas Wireless Propag. Lett.*, vol. 17, no. 1, pp. 110–113, Jan. 2018.

[29] G.-T. Chen, Y.-C. Jiao, and G. Zhao, "A reflectarray for generating wideband circularly polarized orbital angular momentum vortex wave," *IEEE Antennas Wireless Propag. Lett.*, vol. 18, no. 1, pp. 182–186, Jan. 2019.

[30] X. Meng, J. Wu, Z. Wu, T. Qu, and L. Yang, "Dual-polarized reflectarray for generating dual beams with two different orbital angular momentum modes based on independent feeds in C- and X-bands," *Opt. Express*, vol. 26, no. 18, pp. 23185–23195, Sep. 2018.

[31] Y. Zhang, Y. Lyu, H. Wang, X. Zhang, and X. Jin, "Transforming surface wave to propagating OAM vortex wave via flat dispersive metasurface in radio frequency," *IEEE Antennas Wireless Propag. Lett.*, vol. 17, no. 1, pp. 172–175, Jan. 2018.

[32] X.-S. Meng, J.-J. Wu, Z.-S. Wu, T. Qu, and L. Yang, "Design of multiple-polarization reflectarray for orbital angular momentum wave in radio frequency," *IEEE Antennas Wireless Propag. Lett.*, vol. 17, no. 12, pp. 2269–2273, Dec. 2018.

[33] D. Zhang, X. Cao, H. Yang, J. Gao, and X. Zhu, "Multiple OAM vortex beams generation using 1-bit metasurface," *Opt. Express*, vol. 26, no. 19, pp. 24804–24815, Sep. 2018.

[34] F. Qin, L. Wan, L. Li, H. Zhang, G. Wei, and S. Gao, "A transmission metasurface for generating OAM beams," *IEEE Antennas Wireless Propag. Lett.*, vol. 17, no. 10, pp. 1793–1796, Oct. 2018.

[35] H.-F. Huang and S.-N. Li, "High-efficiency planar reflectarray with small-size for OAM generation at microwave range," *IEEE Antennas Wireless Propag. Lett.*, vol. 18, no. 3, pp. 432–436, Mar. 2019.

[36] J. Wu, Z. Zhang, X. Ren, Z. Huang, and X. Wu, "A broadband electronically mode-reconfigurable orbital angular momentum metasurface antenna," *IEEE Antennas Wireless Propag. Lett.*, vol. 18, no. 7, pp. 1482–1486, Jul. 2019.

[37] D. Zhang, X. Cao, J. Gao, H. Yang, W. Li, T. Li, and J. Tian, "A shared aperture 1 bit metasurface for orbital angular momentum multiplexing," *IEEE Antennas Wireless Propag. Lett.*, vol. 18, no. 4, pp. 566–570, Apr. 2019.

[38] Y. Shuang, H. Zhao, W. Ji, T. J. Cui, and L. Li, "Programmable high-order OAM-carrying beams for direct-modulation wireless communications," *IEEE J. Emerg. Sel. Topics Circuits Syst.*, vol. 10, no. 1, pp. 29–37, Mar. 2020.

[39] A. Kumar and G. Singh, "Measurement of dielectric constant and loss factor of the dielectric material at microwave frequencies," *Prog. Electromagn. Res.*, vol. 69, pp. 47–54, Jan. 2007.

[40] *MACOM Technology Solutions, Solderable GaAs Constant Gamma Flip-Chip Varactor Diode*, document MAVR-000120-1411, Dec. 2019. [Online]. Available: http://www.macom.com/products/product-detail/MAVR-000120-14110P

[41] T. Sleasman, M. F. Imani, J. N. Gollub, and D. R. Smith, "Microwave imaging using a disordered cavity with a dynamically tunable impedance surface," *Phys. Rev. A, Gen. Phys.*, vol. 6, no. 5, Nov. 2016, Art. no. 054019.

**KAI GUO** received the B.S. degree in applied physics and the Ph.D. degree in physics from the Harbin Institute of Technology, Harbin, China, in 2010 and 2015, respectively. From 2015 to 2016, he was a Postdoctoral Research Fellow with Sungkyunkwan University, Suwon, South Korea. From 2016 to 2017, he was a Postdoctoral Research Fellow with The Hong Kong Polytechnic University, Hong Kong, China. He is currently working as an Assistant Professor with the Hefei University of Technology, Hefei, China. His research interests include theoretical surface plasmonics, orbital angular momentum (OAM) antenna, OAM communication, light manipulation with metamaterials and metasurfaces, and nonlinear optics.

**QUN ZHENG** received the B.S. degree in communication engineering from Anhui Normal University, Wuhu, China, in 2017. She is currently pursuing the M.S. degree with the Advanced Electromagnetism Function Laboratory (AEMFLab), Hefei University of Technology. Her research interests are mainly in the metasurface and vortex electromagnetic waves.

**ZHIPING YIN** (Member, IEEE) was born in Hunan, China, in 1980. He received the B.Eng. degree in electronic engineering and the Ph.D. degree in electromagnetic field and microwave technology from the University of Science and Technology of China (USTC), Hefei, China, in 2003 and 2008, respectively. From 2009 to 2010, he held a postdoctoral position with the Microwave and Millimeter-wave Engineering Research Center, Department of Electronic Engineering and Information Science, USTC. He is currently a Professor with the Academy of Photoelectric Technology, Hefei University of Technology, Hefei. His current research interests include microwave and terahertz device, phased-array antenna, and microwave imaging radar.

**ZHONGYI GUO** received the bachelor's degree from the Department of Physics, Harbin Institute of Technology, in 2003, and the master's and Ph.D. degrees from the Harbin Institute of Technology, in 2005 and 2008, respectively. From 2008 to 2009, he worked as an Assistant Professor with the Department of Physics, Harbin Institute of Technology. He held a postdoctoral position with Hanyang University, South Korea, for a period of two years. In 2011, he held a postdoctoral position with The Hong Kong Polytechnic University, for a period of six months. He joined the School of Computer and Information, Hefei University of Technology, as a Full Professor, in the end of 2011. His current research interests are in the fields of advanced optical communication, orbital angular momentum antenna, polarization information processing, manipulation of optical fields, and nanophotonics.

● ● ●